N O T I C E

THIS DOCUMENT HAS BEEN REPRODUCED FROM MICROFICHE. ALTHOUGH IT IS RECOGNIZED THAT CERTAIN PORTIONS ARE ILLEGIBLE, IT IS BEING RELEASED IN THE INTEREST OF MAKING AVAILABLE AS MUCH INFORMATION AS POSSIBLE

SQT

NASA CONTRACTOR
REPORT

NASA CR-150632

(NASA-CR-150632) EXTENSIONS TO ANALYSIS OF IGNITION TRANSIENTS OF SEGMENTED ROCKET MOTORS Final Report (Princeton Univ., N. J.) 38 p HC A03/MF A01 CSCL 21H

N82-20241

Unclas
G3/20 09364

EXTENSIONS TO ANALYSIS OF IGNITION TRANSIENTS OF SEGMENTED ROCKET MOTORS

By Leonard H. Caveny
Princeton University
Princeton, New Jersey 08540

6 January 1978

Final Report

Prepared for

NASA-GEORGE C. MARSHALL SPACE FLIGHT CENTER
Marshall Space Flight Center, Alabama 35812

TECHNICAL REPORT STANDARD TITLE PAGE

1. REPORT NO.	2. GOVERNMENT ACCESSION NO.	3. RECIPIENT'S CATALOG NO.
NASA CR-150632		

4. TITLE AND SUBTITLE	5. REPORT DATE
Extensions to Analysis of Ignition Transients of Segmented Rocket motors	6 January 1978
	6. PERFORMING ORGANIZATION CODE

7. AUTHOR(S)	8. PERFORMING ORGANIZATION REPORT #
Leonard H. Caveny	

9. PERFORMING ORGANIZATION NAME AND ADDRESS	10. WORK UNIT NO.
Princeton University Princeton, New Jersey 08540	11. CONTRACT OR GRANT NO. H-30539B

12. SPONSORING AGENCY NAME AND ADDRESS	13. TYPE OF REPORT & PERIOD COVERED
National Aeronautics and Space Administration Washington, D. C. 20546	Contractor Report Final
	14. SPONSORING AGENCY CODE

15. SUPPLEMENTARY NOTES

16. ABSTRACT

The analytical procedures described in NASA CR-150162 were extended for the purpose of analyzing the data from the first static test of the Solid Rocket Booster for the Space Shuttle. The component of thrust associated with the rapid changes in the internal flow field was calculated. This dynamic thrust component was shown to be prominent during flame spreading. An approach was implemented to account for the close coupling between the igniter and head-end segment of the booster. The tips of the star points were ignited first, followed by radial and longitudinal flame spreading.

17. KEY WORDS	18. DISTRIBUTION STATEMENT
	Unclassified-Unlimited A. A. McCool Director, Structures & Propulsion Lab.

19. SECURITY CLASSIF. (of this report)	20. SECURITY CLASSIF. (of this page)	21. NO. OF PAGES	22. PRICE
Unclassified	Unclassified	38	NTIS

NASA - Form 3292 (May 1969)

ACKOWLEDGEMENT

The author expresses appreciation to personnel at the George C. Marshall Space Flight Center and the Wasatch Division of the Thiokol Corporation whose input materially aided this project and, in particular, to B. W. Shackelford, Jr. (NASA Project Coordinator) who provided overall technical guidance.

This project applied and extended analytical techniques developed at the Guggenheim Laboratories of Princeton University under a series of NASA Grants. Accordingly, it incorporates some of the results the author obtained in a previous collaboration with A. Peretz, K. K. Kuo and M. Summerfield.

This project was carried under NASA/MSFC Requisition 1-8-EP-08384 by the author working as a consultant to Princeton Resources, Inc., P.O. Box 211, Princeton, NJ 08540.

TABLE OF CONTENTS

INTRODUCTION

This document describes the results of a small project to extend and apply the analytical techniques (described in Ref. 1) which were developed under a previous NASA contract to predict the ignition and performance transients of segmented, solid propellant boosters. In particular, the project was directed at developing techniques for analyzing the data from the first static test of the Solid Rocket Booster (SRB) for the Space Shuttle (i.e., DM1) and predicting the performance of the second static test, DM2.

The previous study (Ref. 1) developed analytical techniques for the type of segmented motor configuration and ignition events illustrated in Fig. 1. This was accomplished by accounting for (1) the temporal and spatial development of the flow field in segmented motors set up by the igniter discharge, (2) ignition and flame spreading coupled to the main chamber and slot flows, (3) the large velocity, pressure, and temperature gradients that occur during the early phases of ignition, and (4) the interactions that combine to produce peak pressures, (e.g., gas flow into and out of the slots, compression of chamber gases during pressurization, erosive burning, and mass-added effect of igniter discharge).

The work to be summarized in this report has been catagorized as follows:

1) Analysis and prediction of thrust dynamics during flame spreading and chamber pressurization.
2) Extensions to account for the close coupling between the igniter and the head-end segment of the Space Shuttle SRB.
3) General improvements and extensions to the computer program to facilitate parametric studies.

As the pursuit of higher performance rocket motors continues and the present configurations are upgraded (i.e., by increasing loading density, using high-performance propellant, and extending ambient temperature range), the methods extended during the project will enable analysts to predict items such as ignition delays, rate of thrust increase and maximum pressures with much greater confidence than was heretofore possible.

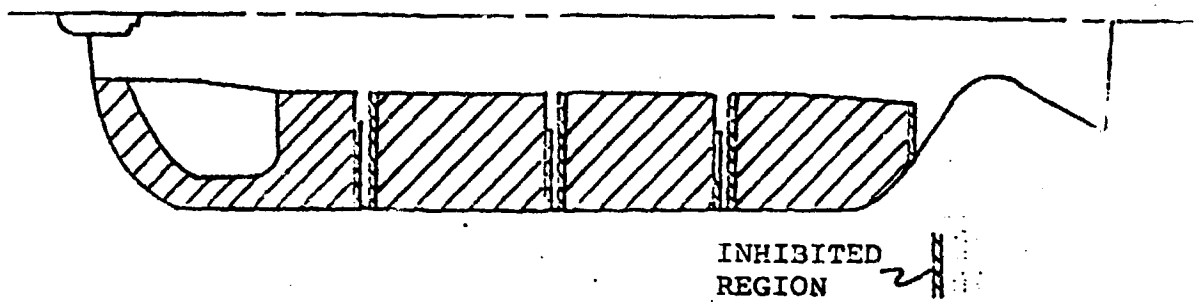

(a) Segmented rocket motor configuration

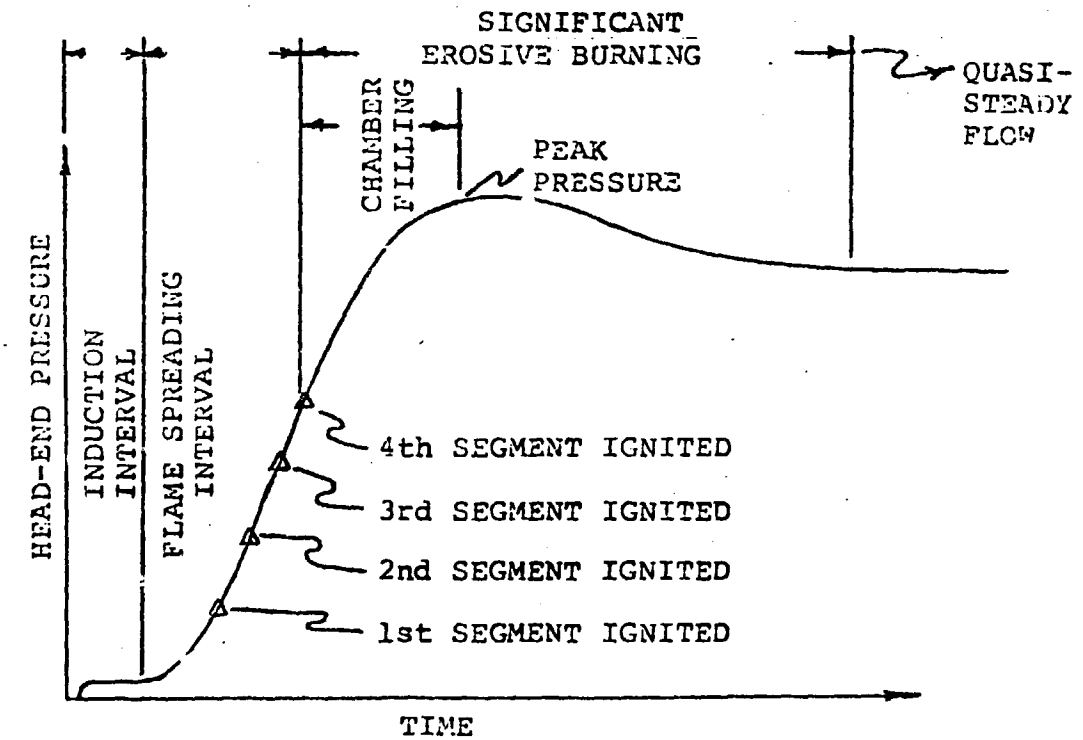

(b) Significant ignition intervals.

Fig. 1 Type of rocket motor and time intervals considered during study.

DYNAMIC THRUST DURING IGNITION TRANSIENTS

Physical Situation Being Analyzed

Rocket motor thrust is the net force exerted by the gases flowing in the rocket motor on the internal solid surfaces. Thrust can be calculated by either summing the resultant forces on the solid surfaces or by finding the change of momentum of the combustion gases in the chamber.

In this discussion, a distinction is made between static thrust and dynamic thrust. Static thrust is the widely used conventional concept of thrust produced by gases flowing through a rocket motor nozzle. Static thrust is usually expressed as

$$F_{noz} = C_{F\lambda m} p_{E,stag} A_t \qquad (1)$$

where A_t is the throat area, $p_{E,stag}$ the stagnation pressure at the nozzle end of the chamber, and $C_{F\lambda m}$ is a coefficient which accounts for the change of momentum as the gases flow from the chamber to the nozzle exit plane. The concepts of calculating $C_{F\lambda m}$ so as to account for divergence losses, flow losses, flow separation, expansion ratio, etc., are well documented in books on propulsion. Static thrust is associated with quasi-steady flow; even though chamber pressure or throat area may be changing rather rapidly, the flow fields in the chamber and nozzle are usually considered to be a series of steady states. Thus, static thrust is based usually on a series of instantaneous values of $p_{E,stag}$ and A_t. The concepts of dynamic thrust are rarely considered and not included in any of the standard texts or monographs on rocketry.

Dynamic thrust is that component of total thrust which is produced by such events as rapidly accelerating changes in the internal rocket motor flow field, rapid relative movement of the propellant or inert hardware, sudden changes in flow area (e.g., nozzle removal or vent port opening), and ejection of objects through the nozzle. Dynamic thrust events noticeable on thrust versus time record are often referred to as thrust spikes.

Dynamic thrust is seldom of interest in the applications of conventional rocket boosters and sustainers. The only common rocket motor situation which produces sufficiently rapid changes in the momentum of the internal gases and discernible thrust spikes, is rapid ignition. In special cases, extinguishment by opening the case or by removing the nozzle can produce prominent thrust spikes. For most situations, the total impulses associated with these events are insignificant fractions of the total. Furthermore, because of limitations of thrust stand dynamic responses, thrust measurements during pressurization are usually very inaccurate (e.g., overdamped instrumentation to compensate for thrust stand ringing) and, thus, thrust spikes during ignition are not observed. However, the boosters being developed for the Space Shuttle are sufficiently long that the dynamic thrust events associated with ignition and pressurization transients are discernible. Indeed, the thrust versus time records of the first static test of the Space Shuttle Solid Rocket Booster (DM1) reveal clearly transient forces on the order 300,000 lbf during the first 200 ms of motor operation.

Figure 2 is a plot of the measured thrust versus time record from the first static test of the booster for the Space Shuttle. The several prominent events associated with the initial thrust are indicated. Coinciding with (what is calculated to be) the onset of flame spreading is a rapid increase in thrust. The thrust between 0.02 and 0.1 seconds occurs before flow through the nozzle is established and, thus, is attributed to the momentum changes that occur within the chamber. The periodic disturbances as thrust increases are attributed to wave action within the chamber and to oscillations of the propellant and case masses.

The analysis summarized in this report is part of an effort to explain the observed thrust events. In particular, the analysis is directed at the effects produced by the developing flow field within the chamber. Another group is analyzing the interactions attributable to acceleration of the propellant and the inert parts.

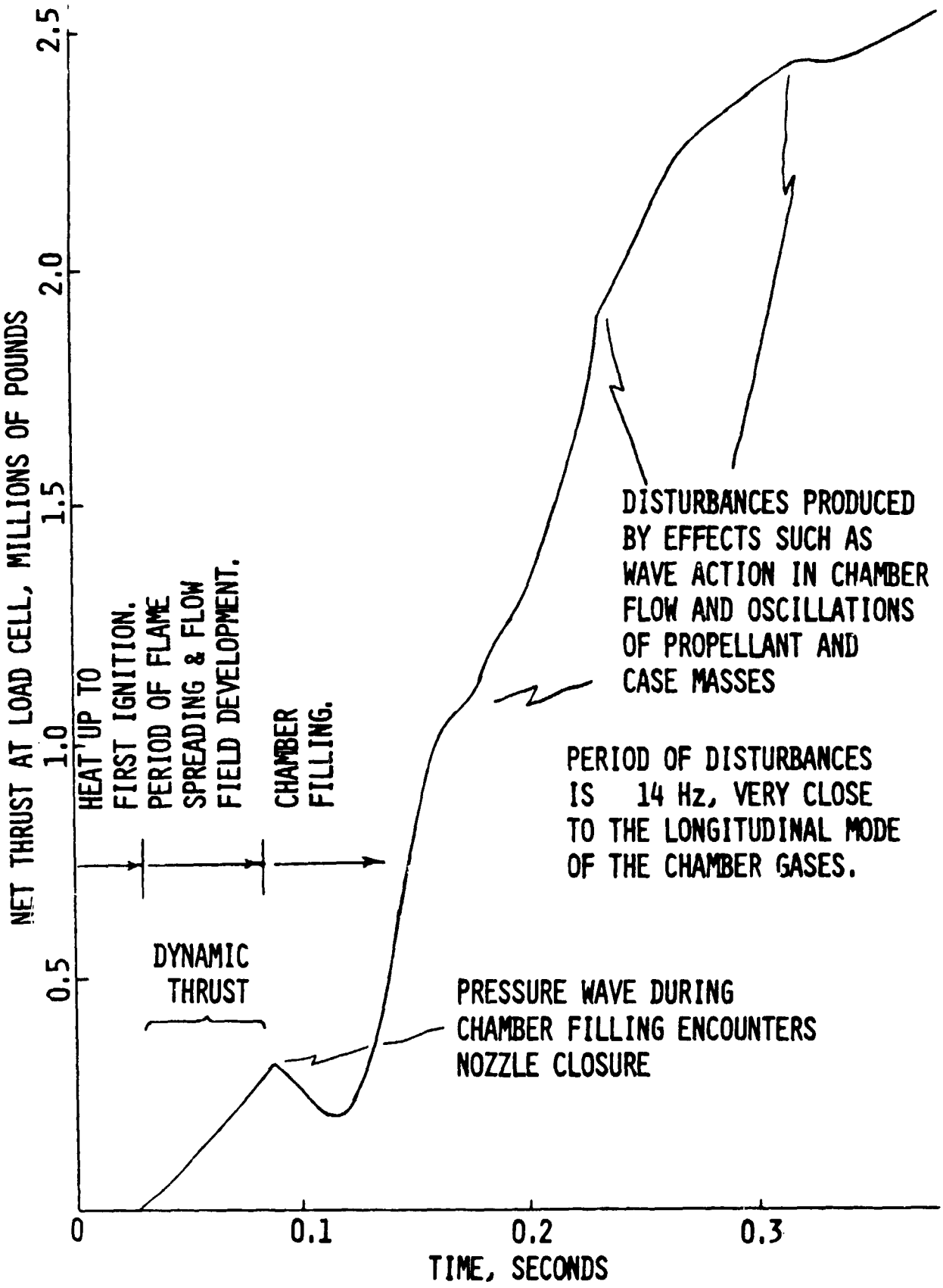

Fig. 2 Dynamic effects noted on plot of measured net thrust versus time for the first static test of the booster for the Space Shuttle (DM1).

General Form of Momentum Equation

In this Section, rather general forms of the momentum relationships are discussed for the purpose of defining those interactions which are pertinent. In the next section, a more manageable set of relationships are applied.

Let $\eta(\vec{x},t)$ be any summable continuous function such as the density ρ, or momentum $\rho\vec{V}$. The "content" of V is $\int \eta dv$. The rate of change with time of that integral is given by Reynold's transport theorem.

$$\frac{d}{dt}\int_{V^*(t)} \eta dv = \int_{V^*(t)} \frac{\partial \eta}{\partial t} dv + \int_{S^*(t)} \eta \vec{b} \cdot \hat{n} dA \qquad (2)$$

d/dt means: following the content within the bounding surface $S^*(t)$ which may move with $\vec{b}(t)$.

$\partial/\partial t$ means: fixing the references in space (relative to inertial frame of reference chosen) and changing with time.

If the control volume chosen is a material volume [i.e., no material element within $S^*(t)$ is ever crossing $S^*(t)$ and $S^*(t)$ is composed of the same material elements throughout the entire time of consideration] instead of d/dt in Eq. (2), write D/Dt to denote material volume and instead of $\vec{b}$, $\vec{u}$ is used. So that

$$\frac{D}{Dt}\int_{V^*(t)} \eta dv = \int_{V^*(t)} \frac{\partial \eta}{\partial t} dv + \int_{S^*(t)} \eta \vec{u} \cdot \hat{n} dA \qquad (3)$$

The momentum balance equation for a material volume is:

$$\underbrace{\frac{D}{Dt}\int_{V^*(t)} \rho\vec{u} dv}_{\text{rate of change of momentum}} = \underbrace{\int_{V^*(t)} \rho\vec{G} dv}_{\text{body force}} + \underbrace{\int_{S^*(t)} \vec{T} dA}_{\text{surface force}} \qquad (4)$$

Now, in the general case, a material volume is not used. Such is the case in thrust calculations. Thus, it is necessary to find the momentum equation in the most general case when the control volume boundary moves with some $\vec{b} \neq \vec{u}$.

Using Reynold's theorems yields:

$$\frac{D}{Dt}\int_{V^*(t)} \rho\vec{u}dv = \int_{V^*(t)} \frac{\partial}{\partial t}(\rho\vec{u})dv + \int_{S^*(t)} (\rho\vec{u}\cdot\vec{u})\cdot\vec{n}dA \qquad (5a)$$

$$\frac{d}{dt}\int_{V^*(t)} \rho\vec{u}dv = \int_{V^*(t)} \frac{\partial}{\partial t}(\rho\vec{u})dv + \int_{S^*(t)} (\rho\vec{u}\cdot\vec{b})\cdot\vec{n}dA \qquad (5b)$$

Though the control volumes' boundaries of Eqs. (5a) and (5b) move with different velocities $\vec{u}$ and $\vec{b}$, at the time of investigation they momentarily coalesce, so that $V^*(t)$ and $S^*(t)$ in Eq. (5a) are identical with $V^*(t)$ and $S^*(t)$ in Eq. (5b).

Summing Eq. (5a) and Eq. (5b) yields:

$$\frac{D}{Dt}\int_{V^*(t)} \rho\vec{u}dv = \frac{d}{dt}\int_{V^*(t)} \rho\vec{u}dv + \int_{S^*(t)} \left(\rho\vec{u}\cdot(\vec{u}-\vec{b})\right)\cdot\hat{n}dA \qquad (6)$$

Note:

$$\frac{D}{Dt}\int_{V^*(t)} \rho\vec{u}dv \neq \frac{d}{dt}\int_{V^*(t)} \rho\vec{u}dv \neq \int_{V^*(t)} \frac{\partial(\rho\vec{u})}{\partial t}dv$$

The reason is that the volumes coincide only at time t, but <u>not</u> at time $t + \Delta t$, see illustration in Fig. 3.

From Eq. (6) and (4)

$$\frac{d}{dt}\int_{V^*(t)} \rho\vec{u}dv + \int_{S^*(t)} \left(\rho\vec{u}\cdot(\vec{u}-\vec{b})\right)\cdot\hat{n}dA = \int_{V^*(t)} \rho\vec{G}dv + \int_{S^*(t)} \vec{T}dA \qquad (7)$$

In the next section, Eqs. (6) and (7) are applied to calculate thrust transients during a static test.

Motor in Thrust Stand

As shown in Fig. 4, the rocket motor is free to move on its stand, exerting its thrust on the load cell which may move some distance ε under the thrust reaction loading. The inertial frame of reference is naturally chosen as the load cell.

t - time

$\vec{x}$ - spatial location

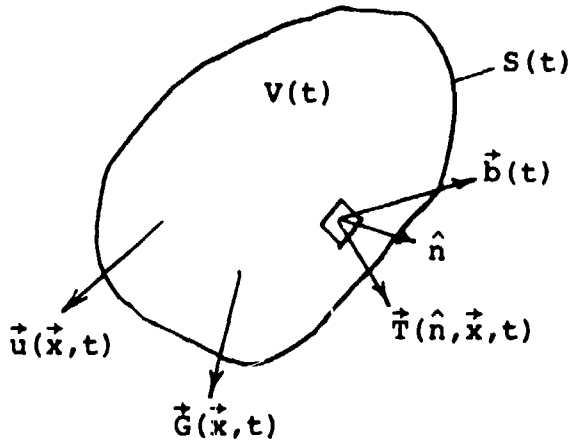

$\vec{u}$ and $\vec{b}$ are measured relative to some inertial frame of reference.

(a) Illustration of parameters used in development of equations.

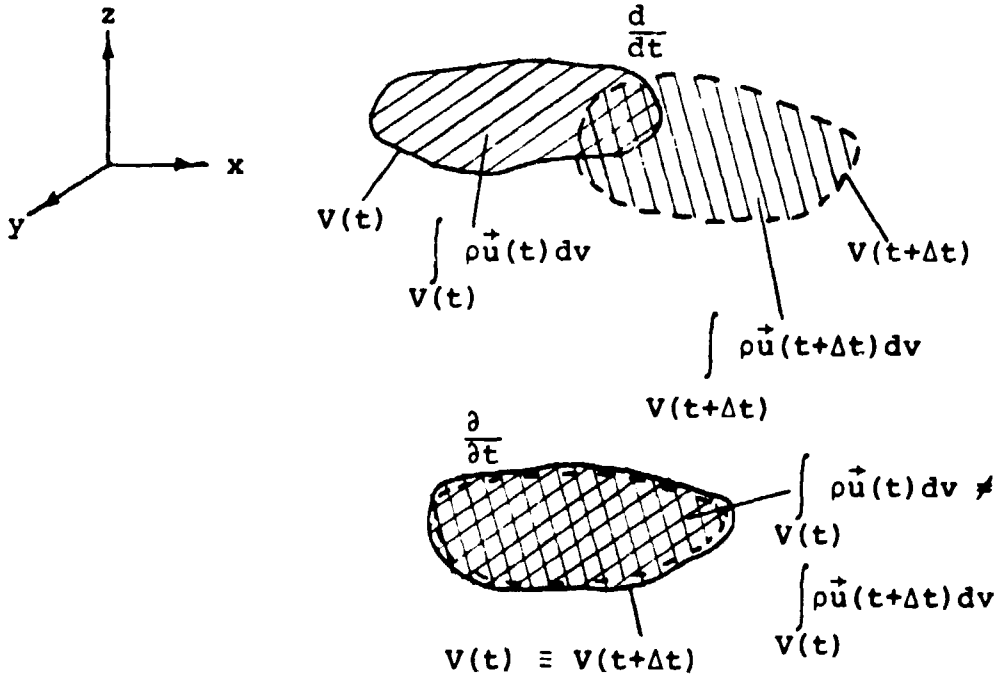

(b) Movement of control volumes.

Fig. 3 General control volumes for development of momentum relationship.

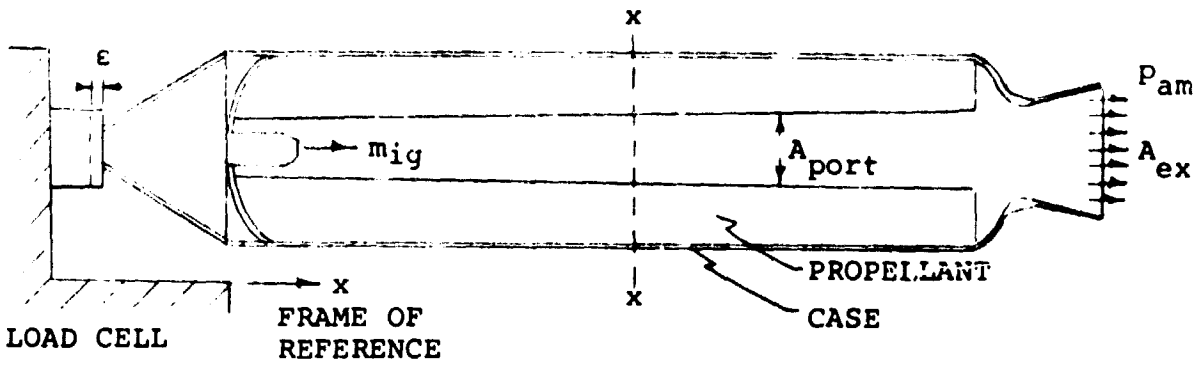

(a) Overall view of motor attached to load cell.

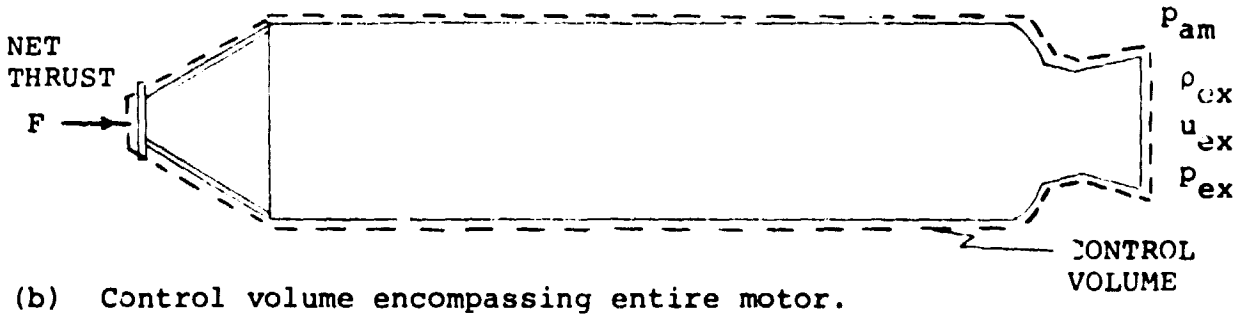

(b) Control volume encompassing entire motor.

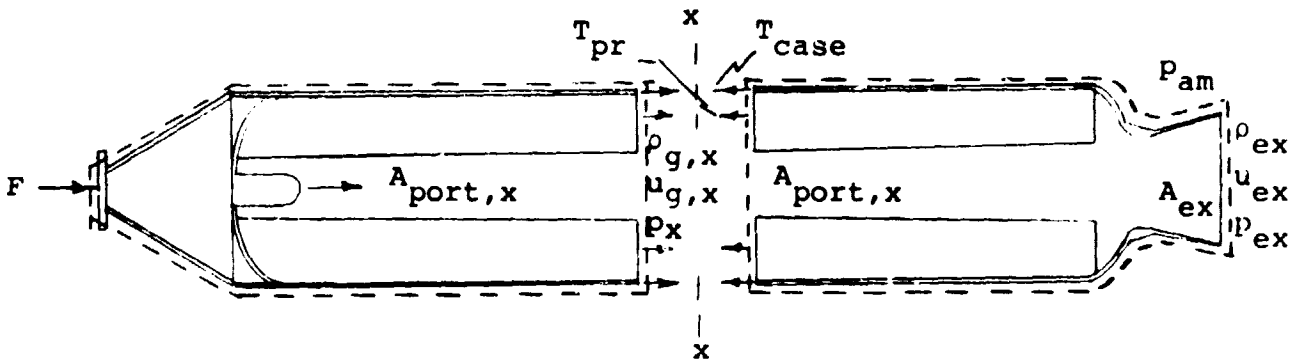

(c) Section through motor revealing stresses in case and propellant.

Fig. 4 Control volumes and nomenclature used in development of dynamic and static thrust relationships.

The control volume is chosen to be the entire rocket motor. Now look at Eq. (7) and identify the various parameters appearing there. Since only the x direction will be considered, the vectorial notation will be dropped.

The following descriptions apply:

b - The control volume boundary velocity relative to the load cell. In this case it is the velocity of the rocket motor outer surface. If the motor case is considered to be rigid, then b is simply the rate at which the motor covers the distance ε.

u - The velocity of any material inside the control volume (relative to the load cell). Conveniently, the velocity of the gas inside the motor is denoted as u_g. The velocities of other components inside will be denoted as:

u_{pr} - propellant segments

u_{case} - motor case segments

It should be emphasized that due to elasticity $u_{pr} \neq u_{case} \neq b$ and also u_{pr} and $u_{case} << u_g$. Since ε is very small, $b << u_g$. Note that u_g, u_{pr}, u_{case}, b are functions of x and t and are taken positive if in the +x direction and negative if in the -x direction.

G - Gravity, is zero in the x direction.

T - The outer pressure force resultant in the x direction.

Now look at each of the terms in Eq. (7). The symbols ρ_g, ρ_{pr}, ρ_{case} are used for denoting densities of the gas, propellant, and case segments inside the control volume. In the sections of the control volume where there are no solid propellant segments, $\rho_{pr} = 0$. Where there is no motor case, $\rho_{case} = 0$ and so on (e.g., in the port area section $\rho_{case} = \rho_{pr} = 0$. On the outer shell, $\rho_g = \rho_{pr} = 0$.) dA in the integrals is taken positive, if $\hat{n}$ is in the x direction, and taken negative if $\hat{n}$ is in the -x direction except in the surface force integral where it is taken always positive. Accordingly, the first term in Eq. (7) becomes

$$\frac{d}{dt}\int_V \rho u dv = \frac{d}{dt}\int_V (\rho_g u_g + \rho_{pr} u_{pr} + \rho_{case} u_{case}) dv \qquad (8)$$

Since $u_g >> b, u_{pr}, u_{case}$, u_g can be taken simply as the value calculated from the set of flow equations inside the motor. Since $\rho_{pr}, \rho_{case} >> \rho_g$, each of the integrands in Eq. (8) may have significant contributions and their relative magnitude should be evaluated before neglecting any of them. Generally, $d/dt \int \rho_g u_g dv$ is the dominant term.

Similarly, the second term in Eq. (7) becomes

$$\int_S \rho u(u-b) dA = \int_S [\rho_g u_g (u_g - b) + \rho_{pr} u_{pr} (u_{pr} - b) + \rho_{case} u_{case} (u_{case} - b)] dA \qquad (9)$$

Obviously, the manner in which the control volume is constructed results in

$$\int_S \rho_{pr} u_{pr} (u_{pr} - b) dA = 0 \qquad (10)$$

(i.e., no propellant on the boundary $\rho_{pr} = 0$).

$$\int_S \rho_{case} u_{case} (u_{case} - b) dA = 0 \qquad (11)$$

(i.e., boundary is composed of motor case).

$$\int_S \rho_g u_g (u_g - b) dA \simeq \rho_{ex} u_{ex}^2 A_{ex} \qquad (12)$$

(i.e., only at the exit plane $\rho_g \neq 0$ and, generally, $u_g >> b$. So that Eq. (9) reduces to

$$\int_S \rho u(u - b) dA = \rho_{ex} u_{ex}^2 A_{ex} \qquad (13)$$

Furthermore, considering the third term in Eq. (7),

$$\int_V \rho G dv = 0 \qquad (14)$$

since gravity is zero in the x direction.

Finally, the remaining term in Eq. (7) can be simplified,

$$\int_S TdA = -p_{ex}A_{ex} + p_{am}A_{ex} + F \qquad (15)$$

Thus, the idealized thrust equation which accounts for dynamic thrust is:

$$F = \frac{d}{dt}\int_V (\rho_g u_g + \rho_{pr} u_{pr} + \rho_{case} u_{case})dv + \rho_{ex} u_{ex}^2 A_{ex} + p_{ex}A_{ex} - p_{am}A_{ex} \qquad (16)$$

The integral on the right hand side of Eq. (16) is the dynamic contribution to thrust F_{dyn}; the remaining terms are the conventional nozzle thrust usually expressed as F_{noz}.

Numerically the above integral should be computed as follows: the momentary volume $V(t)$ is divided into N stations and the increment of time is Δt. Then,

$$\frac{d}{dt}\int_V (\rho_g u_g + \rho_{pr} u_{pr} + \rho_{case} u_{case})dv =$$

$$\left[\sum_{i=1}^{N}\left(\rho_g u_g + \rho_{pr} u_{pr} + \rho_{case} u_{case}\right)_i dv_i\right]_{t+\Delta t} \Big/ \Delta t -$$

$$\left[\sum_{i=1}^{N}\left(\rho_g u_g + \rho_{pr} u_{pr} + \rho_{case} u_{case}\right)_i dv_i\right]_{t} \Big/ \Delta t \qquad (17)$$

Since the values of u_{pr} and u_{case} are not known at this time and since the primary purpose of this analysis is to account for the gas flow effects, the calculations of dynamic thrust in the ignition transients computer program are carried out using a simplified form of Eq. (11).

$$F_{dyn} = \frac{\left[\sum_{i=1}^{N}(\rho_g u_g A_{port})_i \Delta x\right]_{t+\Delta t} - \left[\sum_{i=1}^{N}(\rho_g u_g A_{port})_i \Delta x\right]_t}{\Delta t}$$

The thrust associated with the nozzle is calculated using the

conventional nozzle thrust prediction procedures for quasi-steady flow. Thus, the net thrust is

$$F = F_{dyn} + C_{F\lambda m} p_{E,stag} A_t$$

Discussion of Considering a Partial Control Volume

The motor is now cut at the plane x - x. The main difference in the calculation is the considerations of the tensions (T_{case} and T_{pr}) which may amount to an important part of the total F and should not be neglected unless $u_{g,x}$, p_x, b_x, $u_{pr,x}$, $u_{case,x}$ are zero. Following the reasoning as before we obtain:

Segment A:

$$F = \frac{d}{dt} \int_{V_A} (\rho_g u_g + \rho_{pr} u_{pr} + \rho_{case} u_{case}) dv + \rho_{g,x} u_{g,x}^2 A_{port,x} +$$

$$p_x A_{port,x} - p_{am} A_{xx} - T_{case} - T_{pr} \qquad (18)$$

Segment B:

$$T_{case} + T_{pr} + \frac{d}{dt} \int_{V_B} (\rho_g u_g + \rho_{pr} u_{pr} + \rho_{case} u_{case}) dv - \rho_{g,x} u_{g,x}^2 A_{port,x}$$

$$-p_x A_{port,x} + p_{am}(A_{xx} - A_{ex}) + p_{ex} A_{ex} + \rho_{ex} u_{ex}^2 A_{ex} = 0 \qquad (19)$$

It is easily seen that the summation of Eq. (18) and Eq. (19) yields Eq. (16).

During ignition period of a long motor, cross section x - x can be found where $u_{g,x} = 0$ and $p_x = p_{am}$ and, therefore, $p_{ex} = p_{am}$, $u_{ex} = 0$. Thus, Eq. (19) reduces to:

$$T_{case} + T_{pr} + \frac{d}{dt} \int (\rho_{pr} u_{pr} + \rho_{case} u_{case}) dv + p_{am}(A_{xx} - A_{port,x}) = 0$$

Substituting in Eq. (18) yields:

$$F = \frac{d}{dt} \int_{V_A} (\rho_g u_g + \rho_{pr} u_{pr} - \rho_{case} u_{case}) dv + \frac{d}{dt} \int_{V_B} (\rho_{pr} u_{pr} + \rho_{case} u_{case}) dv$$

If $V_A >> V_B$, i.e., $x - x$ is close to the nozzle, we can calculate F considering only Segment A and using a reduced Eq. (18).

$$F = \frac{d}{dt} \int_{V_A} (\rho_g u_g + \rho_{pr} u_{pr} + \rho_{case} u_{case}) dv$$

Generally, however, the thrust reaction F cannot be calculated considering a partial control volume like Segment A because T_{case} and T_{pr} are unknown.

EXTENSION TO COMPUTER PROGRAM

In the subsections that follow, the modifications to the program and the new input and output are described in modular form. The descriptions follow the formats used in Ref. 1. The new computer program is designated as HVTSEG2. Table 1 is an input data set for an example case.

In the extended version of the program the subroutine TIMEST was eliminated and its function is now performed by MAIN. The subroutine FCT was eliminated since it dealt with a particular slot flow option which was found to be unrealistic, i.e., large pressure differentials between the main chamber and slots do not occur in the SRB. A multi-point interpolation subroutine, ITERP1, was added as part of the procedure for calculating thrust differentials.

Although numerous changes and improvements have been made to the Ref. 1 computer program, the input data decks from the Ref. 1 version of the program can be used without change.

The following changes to Section 4 of Ref. 1 should be noted:

pg. 47 - Delete XG as an input. The program sets $XG = XE - \Delta x/2$.

- Add to description of TIGN: Corrected by program whenever TPI $\neq$ TOREF.

pg. 48 - Delete DDHC as an input. The factor multiplying the heat transfer coefficient is now CHC(N).

pg. 49 - The first two lines should be changed to:

or by a table

$$r_0 = f(p)\ \exp[\sigma_p(T_{pi} - T_{0,ref})] \qquad (4\text{-}2)$$

Ignition of First Segment in Space Shuttle SRB

The large surface area associated with the head-end segment of the Space Shuttle SRB produces a rather unusual ignition sequence. Once the head-end pyrogen ignites the head-end segment, the mass flux from the head-end segment dominates the mass flux from the pyrogen by more than 7 to 1. Thus, the head-end segment is effectively the igniter for the remaining segments. Accordingly, predictions of the start-up transients and parametric studies to tailor the start-up thrust versus time program, require that careful attention be given to the ignition of the head-end segment.

In the current design of the Space Shuttle SRB, the nozzle of the igniter is very close to the star-point tips in the first segment. It has been pointed out[2] that treating the head-end region as a uniformly heated port (as in the Ref. 1 analysis) results in unrealistically long induction periods. A better simulation will be obtained by considering at least three zones of heating and ignition in the first segment: (1) the more intense heating, rapid ignition, and high rate of flame spreading of the star-point tips, (2) the increasing heating rate and flame spreading rate in the axial slots as the gas generated by the burning star-point tips augments the axial flow of hot gases, and (3) the conventional heating of the aft portion of the first segment. Thus, the net effect will be to reduce the predicted induction time and to extend the flame spreading interval for the first segment. Recall that the results of Ref. 1 showed that flame spreading rate (downstream of the first increment) is relatively insensitive to the propellant property changes, whereas time to first ignition is affected greatly by small variations in the ignition criterion and heat flux. Accordingly, an important extension to the computer program was to include the capability of treating more completely the specifics of the igniter discharge pattern and propellant surface geometry in the head-end segment.

Corrections for Changes in Initial Temperature*

The program input should be prepared by considering the following inputs to be determined at the temperature, $T_{0,ref}$:

TIGN = T_{ig}
TFREF = $T_{f,ref}$
RREF = r_{ref}
TIGTAB & MIGTAB
PDATA & RDATA

When the input initial temperature (or ambient temperature) T_{pi} differs from $T_{0,ref}$, the following corrections are made to account for the temperature differential, $\Delta T_0 = T_{pi} - T_{0,ref}$

$$T_{ig}@T_{pi} = T_{ig} + (c_{pr}/c_{ch})\Delta T_0$$

$$T_f@T_{pi} = T_{f,ref} + (c_{pr}/c_{ch})\Delta T_0$$

$$r@T_{pi} = r_{ref} \exp(\sigma_p \Delta T_0)$$

$$TIGTAB@T_{pi} = TIGTAB/\exp(\pi_k \Delta T_0)$$

$$MIGTAB@T_{pi} = MIGTAB \exp(\pi_k \Delta T_0)$$

$$r@T_{pi} = f(PDATA,RDATA)\exp(\sigma_p \Delta T_0)$$

All of these corrections can be suppressed by inputting <u>all</u> of the values at the desired temperature, T_{pi}, and inputting $T_{0,ref} = T_{pi}$.

The burning rate corrections can be eliminated by inputting $\sigma_p = 0.0$.

The corrections to the igniter mass flow rate table can be eliminated by inputting $\pi_k = 0.0$.

---

*It is assumed that the reader is familiar with nomenclature and input description of Ref. 1.

Special Input for Control of Flame Spreading

Time of ignition and flame spreading rate after first ignition can be studied parametrically by invoking special inputs. Since the heat transfer coefficient at each station can be adjusted individually, the time of first ignition can be controlled. Also, the fraction of each axial station that is ignited initially can be prescribed. At each axial station*, during flame spreading

$$b = p_w[b_{fl} + (1 - b_{fl})/\Delta t_{ff}]$$

When flame spreading is complete,

$$b = p_w$$

The heat transfer coefficient at each station is the value calculated by the empirical equation multiplied by

$$C_{h,n}$$

The following inputs can be prescribed for each axial station, from 0 to NDELX:

CHC(N)	$C_{h,n}$	A factor multiplying the heat transfer coefficient for the purpose of providing a prescribed adjustment at each individual axial station. The input DDHC (a constant multiplier for all stations) is replaced by $C_{h,n}$. (1.0)	
BFl(N)	$b_{fl,n}$	The fraction of the perimeter which burns following first ignition. (1.0)	
DELTTF(N)	$\Delta t_{ff,n}$	Time required for flame to spread over remaining perimeter, i.e., the fraction $1 - b_{fl,n}$. Cannot be zero. (1.0)	s

*Note that in the extended version of the program the burning perimeter is printed out as zero until ignition occurs and then the time-dependent output of burning perimeter reveals how flame spreading within a single increment increases with time.

Special Inputs to Facilitate Parametric Studies

The following inputs are used to extend the output of the program, simplify some of the inputs, and to improve the simulation of actual rocket motors.

Computer Sumbol	*Symbol in Text*	*Description*	*Units*
GAMAN	γ_{noz}	Effective ratio of specific heats of all combustion products in the nozzle. ($\gamma_{noz} = \gamma$)	
PISUBK	π_k	Temperature sensitivity of pressure and burning time of igniter, for corrections from $T_{0,ref}$ to T_{pi}. (0.0)	K^{-1}
TIIN	t_{in}	Initial time at which solution begins. (0.0)	s
DELTTF	Δt_F	Thrust differentials between the times t and $t - \Delta t_F$ are calculated at each printout interval for the purpose of examining thrust imbalance between two motors. (0.0)	s
DFSDT	$\Delta t_{\Delta F}$	Thrust increases between the preceding time interval $\Delta t_{\Delta F}$ are calculated at each printout interval for the purpose of examining the rate of thrust increase during pressurization. (0.0)	s

Special Input for Nozzle Closure

The program can approximate the effects produced by using a nozzle closure during the chamber filling phase of ignition. The solution operates on the assumption that the nozzle closure does not completely block the flow at the throat. Thus, there must always be a small vent area in the closure, e.g., 10% of the throat area. For practically all situations, a nozzle closure which blocks 90% of the throat produces pressurization rates which are comparable to a completely blocked throat. Since nozzle closures require a finite time to be carried away, the solution causes the throat area to increase linearly from the small vent area associated with the closure to the final throat area.

The inputs for this option are:

Computer Symbol	*Symbol in Text*	*Description*	*@units CGS(modified)*
POPEN		When POPEN $\leq$ 7776.0, POPEN is considered to be the nozzle-end stagnation pressure at which the nozzle closure begins to carry away. (7777.0)	atm
NBL		(1) Vent area in closure is A_t/NBL and (2) the number of Δt's required to open the discharge area from A_t/NBL to A_t, after the nozzle closure begins to carry away, is NBL*BLANK4. (10)	
BLANK4		The number of time steps required to remove the nozzle closure is NBL*BLANK4. (1.0)	

Special Summary Output

The following time-dependent variables are output in tabular form at intervals NPRINT. British units are used in the summary.

Computer Symbol	*Symbol in Text*	*Description*	*Units*
TI	t	Time	s
PHPSI	p_1	Static pressure at head end of motor.	psia
PEPSI	p_E	Static pressure at nozzle end of propellant grain (or blast tube).	psia
PESTAP	$p_{E,stag}$	Stagnation pressure at nozzle end of motor.	psia
M	M_E	Mach number at nozzle end of propellant grain (or blast tube).	
FLBF	F	Nozzle thrust based only on quasi-steady nozzle flow.	lbf
FDYNLB		Thrust associated with transient chamber flow upstream of nozzle.	lbf
FIMBAL	F_{imbal}	Thrust differential between the times t and $t - \Delta t_f$ (Based on nozzle thrust.)	lbf
FRATE	ΔF in $\Delta t_{\Delta F}$	Thrust increase during the time interval $\Delta t_{\Delta F}$. (Based on nozzle thrust.)	lbf
FMIGLB	m_{ig}	Mass flow rate from igniter.	lbm/s
FNET		Sum of nozzle thrust and dynamic thrust, FLBF + FDYNLB	lbf

The Summary output is set up to be displayed in three forms:

1. at the end of each time-dependent out (i.e., part of the standard listing).
2. as a deck for input to plot programs (i.e., Unit 8 in subroutine ANS is designated SYSOUT = B in the JCL).
3. As a separate listing (see Table 2) following the standard listing (i.e., Unit 9 in subroutine ANS is designated SYSOUT = A in JCL).

The JCL is indicated in Table 1. To suppress punching of card deck, change SYSOUT=B to SYSOUT=DUMMY in JCL.

```
//* DATA TO BE EXECUTED FOLLOWS  GO.SYSIN DD
//GO.FT09F001 DD SYSOUT=A
//GO.FT08F001 DD SYSOUT=B
//GO.SYSIN DD *
 DM1 17DEC77 FLAME SPREAD CONTRO AT HEAD END  ,DYNAMIC THRUST CHECKOUT
 &NAME
      THAX=.002
      TPRINT=.002
      DELTAT=.00016
      NDELX=24
      PAM=.84717
      UNIT=-2.
      AT=2325.81
      XP=2.67
      XF=1329.972
      RUFSUR=0.01
      FKPR=0.0011
      ROPR  =1.7568
      CPR=.3
      SIGP=.0009939
      RREF=1.0540
      PREF=68.08
      BREXP = 0.33
      EBC=0.
      DE=145.64
      CM=.97844
      ALFAD=12.31
      NICTAB=19
      NAPDVX = 25
      DDHC=0.94
      TPI=298.89
      TIGN=2685.4
      TFREF=3353.
      W=28.18
      TPSCRI=850.
      GAMA  =1.1360
      GAMAN =1.1348
      PISUBK=0.0027
      NDATA =3
      DELTTF=0.00906
      DFSDT =0.010
      NBL=10
      BF1= 0.1,0.1,0.1,27*1.0
      CHC= 1.4,1.3,1.2,1.1,26*1.0
      DELTFF= 0.010,0.007,0.005,27*1.
      NPNPXT=2
      NPNPXT=0
 &END
    0.          1.
    0.0200   18.11
    0.0280   46.95
    0.0440   406.05
    0.0520   484.35
    0.0640   514.35
    0.0700   516.69
    0.0880   510.06
    0.1800   427.47
    0.2400   392.42
    0.2880   371.00
    0.3440   348.43
    0.3560   339.86
    0.3800   313.75
```

JCL for Summary table

new

new

Input to control flame spreading

TABLE 1
Input for example case for HVTSEG2

Table 1 (continued)

```
    0.4240   275.18
    0.4600   253.38
    0.5080   232.73
    0.5560   219.50
    0.5600   0.0
     2.67   2538.44   1154.45   1154.45    31.    22939.   59741.    2.21
    57.97   2543.62   1156.49   1156.49
   113.28   2561.7    1144.95   1144.95
   168.58   2706.87    278.93    278.93
   223.89   2612.1     181.18    181.18
   279.19   2645.      182.31    182.31   329.52   877.     20151.    1.5
   334.5    2658.85    182.79    182.79
   389.8    2705.32    184.38    184.38
   445.1    2774.53    186.72    186.72
   500.41   2844.42    189.06    189.06
   555.71   2915.19    191.4     191.4
   611.02   3029.79    195.13    195.13   649.52   2896.    20003.    1.5
   666.32   2757.93    186.16    186.16
   721.63   2720.09    184.88    184.88
   776.93   2789.3     187.22    187.22
   832.23   2859.38    189.56    189.56
   887.54   2930.33    191.89    191.89   942.     3653.    19931.    1.5
   942.84   3072.28    196.49    196.49
   998.15   3025.31    194.98    194.98
  1053.45   3224.03    201.28    201.28
  1108.76   3731.7     216.55    216.55
  1164.06   4316.43    232.9     232.9
  1219.36   4946.2     249.31    249.31   1293.2   15349.   37980.    9.1
  1274.67   5404.35    260.6     260.6
  1329.972  5594.67    265.15    265.15
   0.6808   0.1002
   4.7651   0.4384
  68.08     1.054
  &NAME
       TMAX=.01
       DELFAC=1.3
  &END
  &NAME
       TMAX=.1
       TMAX=0.09
  &END
  &NAME
       TMAX=.12
  DELFAC=.5
       TPRINT=0.001
  &END
  &NAME
       TMAX=.3
       DELFAC=2.
  &END
  &NAME
       TMAX=.4
       TPRINT=.005
       DELFAC=1.
  &END
  &NAME
       TPRINT=.01
       DELFAC=1.
       TMAX=.5
  &END
  &NAME
       TMAX=1.
  &END
```

Table 2 Special summary output table for example case for HVTSEG2.

1 HVT ROCKET MOTOR IGNITION PREDICTION - SEGMENTED - NOV 77
INCLUDES: SPATIAL & TIME DEVELOPMENT OF P,U,&T AND FLAME SPREADING

DM1 17DEC77 FLAME SPREAD CONTRO AT HEAD END ,DYNAMIC THRUST CHECKOUT
**** SUMMARY OUTPUT OF TIME DEPENDENT RESULTS *****

TIME SEC	PHEAD PSIA	PNOZ PSIA	PCNOZ PSIA	MNOZ -	THRUST LBF	FDYN LBF	F IMBAL LBF	F RATE LBF	MIGN LB/S	FNET LBF
0.0002	14.	12.	12.	0.02	0.	0.	0.	0.	17.6	0.
0.0020	15.	12.	12.	0.02	0.	7412.	0.	0.	17.6	74
0.0040	14.	12.	12.	0.02	0.	1636.	0.	0.	17.7	163
0.0060	14.	12.	12.	0.01	0.	1148.	0.	0.	17.7	1148.
0.0080	14.	12.	12.	0.01	0.	1260.	0.	0.	17.8	1260.
0.0100	14.	12.	12.	0.01	0.	1464.	0.	0.	17.9	1.
0.0120	14.	12.	12.	0.01	0.	2166.	0.	0.	17.9	2166.
0.0140	14.	12.	12.	0.01	0.	2149.	0.	0.	18.0	2149.
0.0160	14.	12.	12.	0.01	0.	2163.	0.	0.	18.0	2163.
0.0180	14.	12.	12.	0.01	0.	2202.	0.	0.	18.1	2202.
0.0200	14.	12.	12.	0.01	0.	2262.	0.	0.	18.3	2262.
0.0220	14.	12.	12.	0.01	0.	2865.	0.	0.	25.6	2865.
0.0240	14.	12.	12.	0.01	0.	3064.	0.	0.	32.8	3064.
0.0260	14.	12.	12.	0.01	0.	2864.	0.	0.	40.1	2864.
0.0280	14.	12.	12.	0.01	0.	3296.	0.	0.	48.6	3296.
0.0300	16.	12.	12.	0.01	0.	7460.	0.	0.	93.7	7460.
0.0320	17.	12.	12.	0.01	0.	12499.	0.	0.	138.8	12499.
0.0340	18.	12.	12.	0.01	0.	18309.	0.	0.	183.9	18309.
0.0360	20.	12.	12.	0.01	0.	24627.	0.	0.	229.0	24627.
0.0380	21.	12.	12.	0.01	0.	31141.	0.	0.	274.1	3 141.
0.0400	22.	12.	12.	0.01	0.	37730.	0.	0.	319.2	377 .
0.0420	24.	12.	12.	0.01	0.	44389.	0.	0.	364.3	44389.
0.0440	25.	12.	12.	0.01	0.	51129.	0.	0.	408.1	51129.
0.0460	26.	12.	12.	0.01	0.	55453.	0.	0.	427.7	55453.
0.0480	27.	12.	12.	0.01	0.	58766.	0.	0.	447.4	58766.
0.0500	28.	12.	12.	0.01	0.	61490.	0.	0.	467 1	61490.
0.0520	29.	12.	12.	0.01	0.	63688.	0.	0.	485.8	63688.
0.0540	30.	12.	12.	0.01	0.	63948.	0.	0.	490.9	63948.
0.0560	30.	12.	12.	0.01	0.	63271.	0.	0.	495.9	63271.
0.0580	31.	12.	12.	0.01	0.	62158.	0.	0.	500.9	62158.
0.0600	31.	12.	12.	0.01	0.	61156.	0.	0.	505.9	61156.
0.0620	34.	12.	12.	0.02	0.	61193.	0.	0.	510.9	611
0.0640	37.	12.	12.	0.02	0.	64839.	0.	0.	515.6	64839.
0.0660	43.	12.	12.	0.02	0.	72564.	0.	0.	516.4	72564.
0.0680	56.	12.	12.	0.02	0.	94464.	0.	0.	517.2	94464.
0.0700	73.	12.	12.	0.03	0.	132362.	0.	0.	517.9	132362.
0.0720	92.	12.	13.	0.04	0.	185618.	0.	0.	517.1	185618.
0.0740	109.	13.	13.	0.05	0.	241191.	0.	0.	516.4	241191.
0.0760	125.	13.	13.	0.06	0.	287955.	0.	0.	515.6	287955.
0.0780	143.	13.	13.	0.09	0.	341420.	0.	0.	514.9	341423.
0.0800	161.	13.	13.	0.12	0.	397931.	0.	0.	514.2	397931.
0.0820	178.	14.	14.	0.17	0.	449776.	0.	0.	513.4	449776.
0.0840	193.	15.	15.	0.22	0.	487593.	0.	0.	512.7	487593.
0.0860	205.	18.	18.	0.25	0.	510843.	0.	0.	511.9	510
0.0880	216.	22.	23.	0.26	35699.	521846.	0.	0.	511.1	55754
0.0900	226.	30.	31.	0.26	57143.	521546.	0.	0.	509.3	578620.
0.0910	229.	36.	37.	0.26	73947.	446518.	0.	0.	508.4	520464.
0.0920	232.	45.	47.	0.26	101068.	407510.	0.	0.	507.5	508578.
0.0930	235.	60.	62.	0.26	145021.	357513.	0.	0.	506.6	502534.
0.0940	238.	82.	85.	0.26	216007.	306944.	0.	0.	505.7	522951.
0.0950	242.	115.	119.	0.26	324400.	260417.	0.	0.	504.8	58481
0.0960	246.	158.	164.	0.26	472083.	214675.	0.	0.	503.9	686758.

Table 2 (continued)

0.0970	250.	205.	213.	0.26	639679.	144917.	0.	0.	503.0	784396.
0.0980	254.	245.	254.	0.26	785125.	50012.	0.	0.	502.1	835137.
0.0990	258.	269.	279.	0.26	879787.	-46334.	0.	0.	501.2	833451.
0.1000	262.	275.	285.	0.26	904994.	-103972.	832361.	0.	500.3	[illegible]
0.1010	265.	269.	279.	0.26	882090.	-114840.	783147.	808160.	499.4	767[illegible]50.
0.1020	269.	258.	268.	0.26	837812.	-92064.	696229.	736772.	498.5	745748.
0.1030	273.	247.	256.	0.26	791172.	-57287.	580540.	646196.	497.6	733285.
0.1040	276.	237.	246.	0.26	754806.	-20005.	438104.	538869.	496.7	734801.
0.1050	280.	229.	238.	0.26	727995.	13220.	265436.	403695.	495.8	741215.
0.1060	283.	225.	234.	0.26	712264.	38921.	82323.	240303.	494.9	751185.
0.1070	287.	223.	232.	0.26	706443.	53586.	-71297.	67086.	494.0	760[illegible]30.
0.1080	290.	224.	232.	0.26	707099.	61686.	-168923.	-17933.	493.1	768785.
0.1090	294.	225.	233.	0.26	711502.	66470.	-193333.	-160239.	492.2	777972.
0.1100	297.	227.	236.	0.26	720562.	67614.	-163526.	-184431.	491.3	788176.
0.1110	300.	230.	239.	0.26	731811.	66316.	-108755.	-150305.	490.4	798127.
0.1120	303.	233.	242.	0.26	743140.	65667.	-50569.	-94707.	489.4	808807.
0.1130	307.	237.	246.	0.26	754321.	65808.	-2419.	-36883.	488.5	820129.
0.1140	310.	240.	249.	0.26	765600.	66100.	36294.	10770.	487.6	831700.
0.1150	313.	243.	252.	0.26	777188.	66046.	84253.	69177.	486.7	843234.
0.1160	316.	246.	255.	0.26	789165.	65383.	82558.	76898.	485.8	854548.
0.1170	319.	249.	259.	0.26	802174.	64049.	95192.	95699.	484.9	866193.
0.1180	323.	253.	262.	0.26	816002.	62166.	104900.	108905.	484.0	878168.
0.1190	326.	256.	266.	0.26	830019.	59855.	110069.	118523.	483.1	889[illegible]75.
0.1200	329.	260.	270.	0.26	844202.	57313.	113076.	123648.	482.2	901515.

Note: There are three thrust outputs

FNET = THRUST + FDYN

where THRUST is conventional nozzle thrust
and FDYN is dynamic thrust.

RESULTS FROM EXTENDED PROGRAM

Two sets of calculations were performed for the purpose of demonstrating the features of the extended program:

Case 1 - DM1 17DEC77 FLAME SPREAD CONTROLLED

Input approximates situation for DM1 and the new input parameters (for ignition and flame spreading) were selected to accelerate initial ignition of the first segment and delay the flame spreading along the longitudinal slots of the first segment. Input values are listed in Table 1.

Case 2 - DM1 6JAN78 FLAME SPREAD NOT CONTROLLED

Input is the same as Case 1, except the controls over ignition and flame spreading as imposed by the new input parameters are not invoked, i.e., BF1=30*1.0,CHC=30*1.0,DELTFF=30*1.0

Figures 5 and 6 are normalized plots of the igniter mass flux, pressure rise and thrust events during the induction, flame spreading, and initial pressurization phases. In Case 1, ignition of the starpoint tips occurs more rapidly than the uniform ignition situation in Case 2; thus, head-end pressure begins to rise rapidly, about 0.008 s sooner. However, as shown in Fig. 7, the average flame spreading rate of Case 1 is about 30% slower than Case 2. This may not be a result of the imposed delay in the flame spreading rate of the longitudinal slots, but rather a result of the downstream region not being preheated by the igniter mass flow. However, the slower flame spreading rate of Case 1 does not diminish the strength of the axial pressure wave advancing down the port nor does it diminish the dynamic thrust contribution.

As shown in Figs. 5 and 6, the dynamic thrust contribution is prominent during the time of flame spreading and decays rapidly as the longitudinal pressure wave encounters the aft-end of the motor. Indeed, a sufficiently strong longitudinal pressure wave can produce a negative F_{dyn} as the wave encounters the aft closure. Figure 8 reveals that the time relationship between the igniter flow arriving at the nozzle and the surge of hot gases from the head-end segment

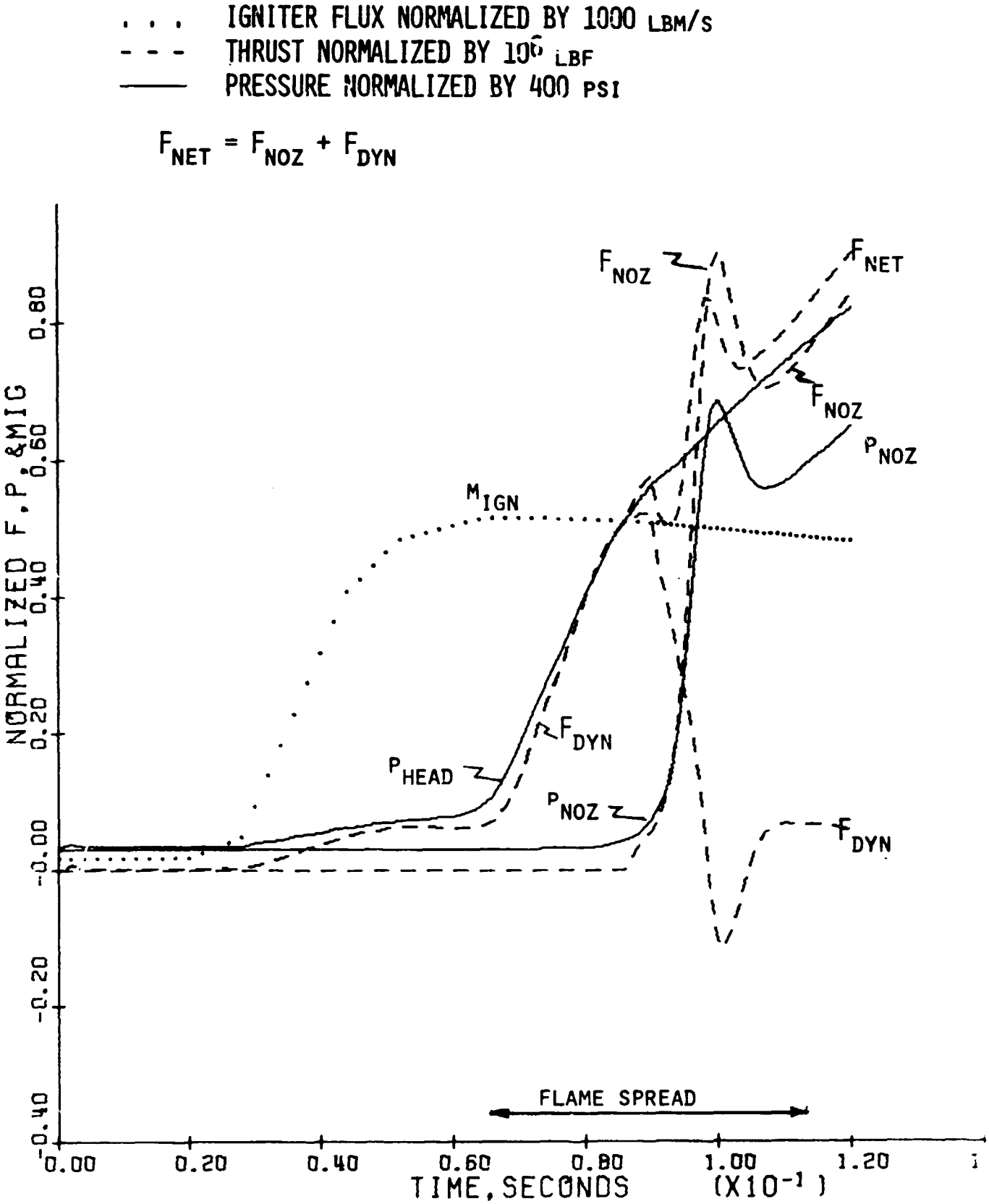

Fig. 5 Igniter mass flux, pressure rise, and thrust events for CASE1 17DEC77 FLAME SPREAD CONTROLLED.

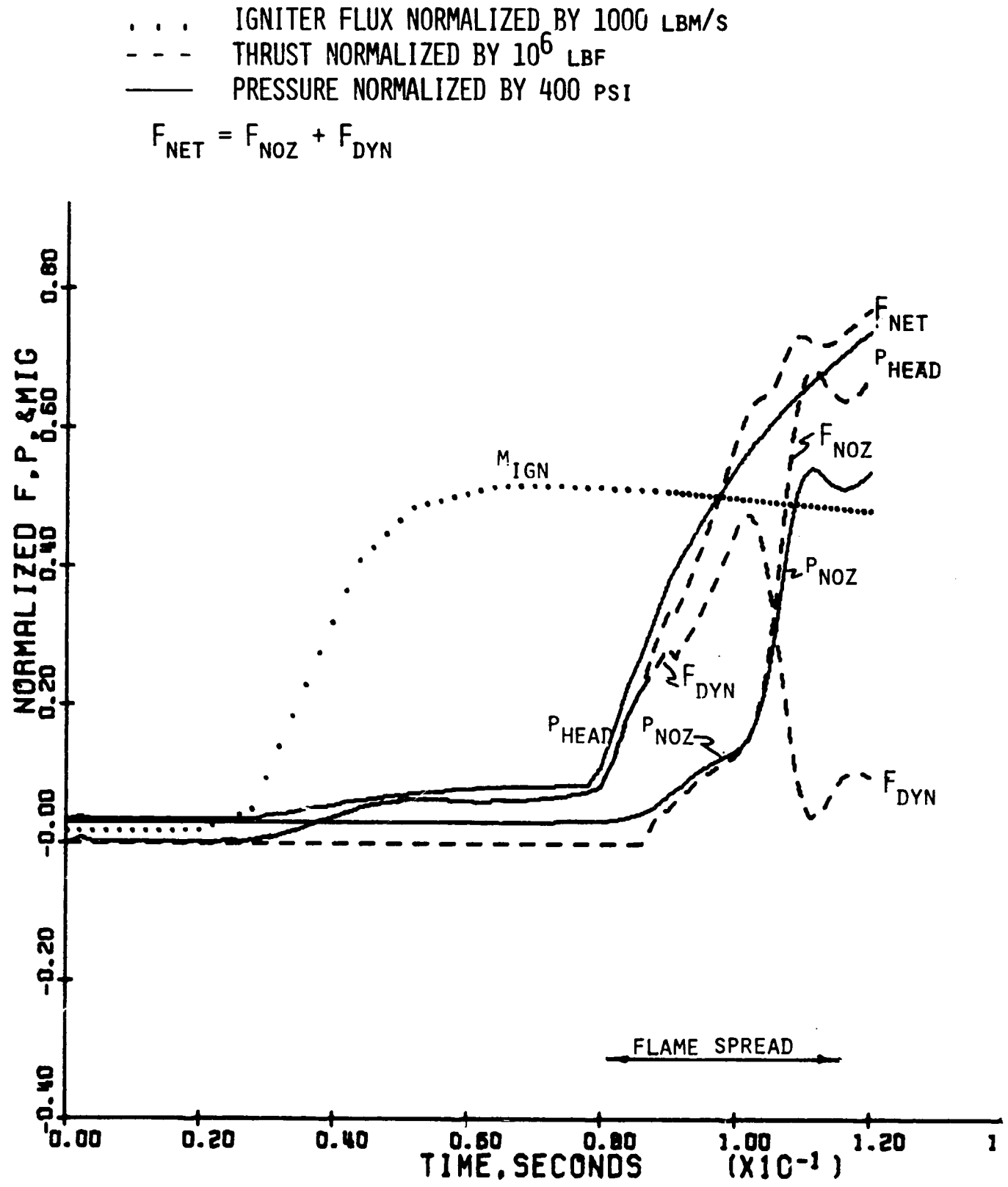

Fig. 6 Igniter mass flux, pressure rise, and thrust events for CASE2 6JAN78 FLAME SPREAD NOT CONTROLLED.

CASE	AVG FLAME SPREAD RATE FT/SEC
1	1990
2	2820

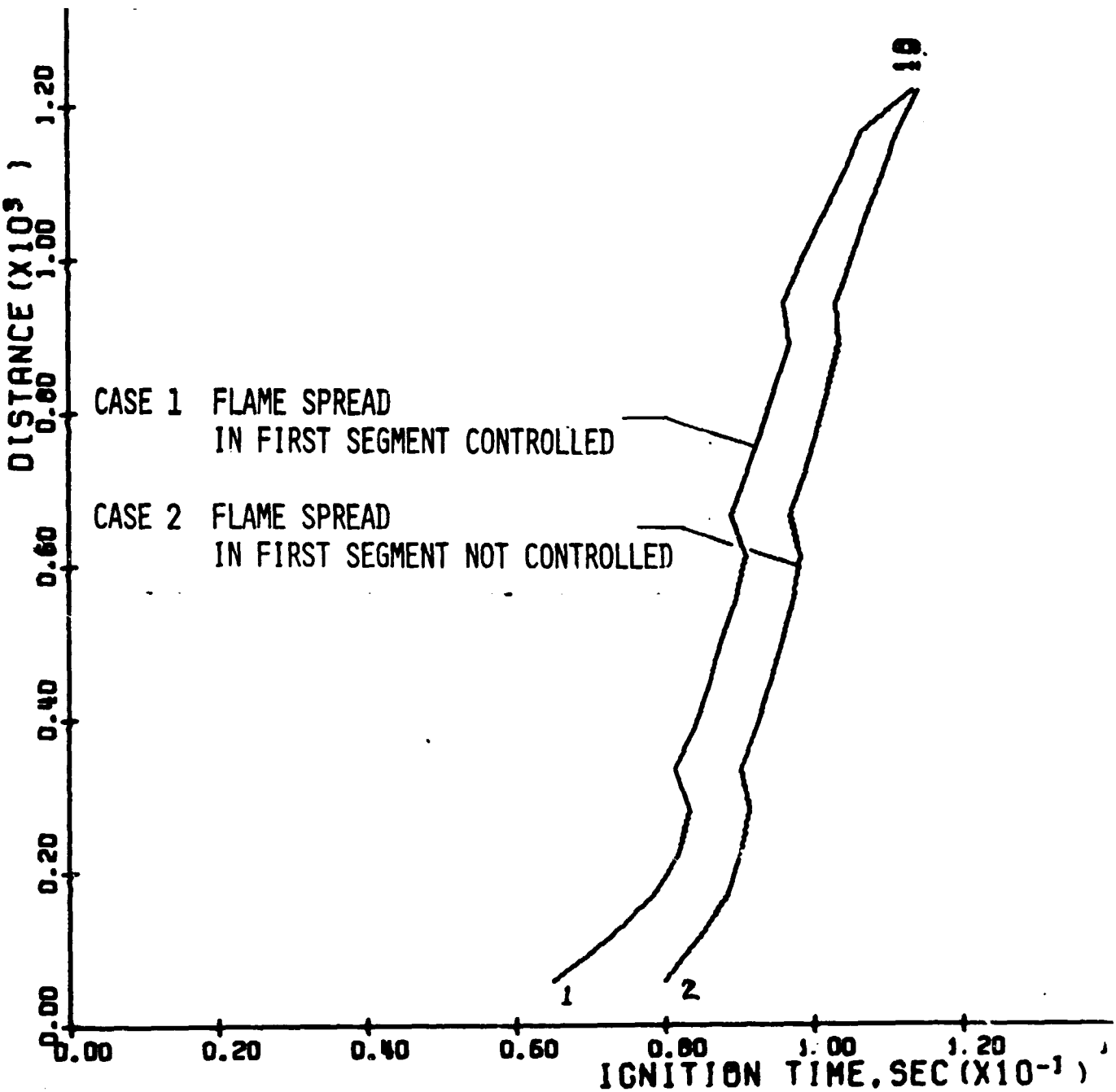

Fig. 7 Flame spreading for CASES 1 and 2 showing that the slower flame spreading rate in the first segment significantly decreases the average flame spreading rate over the length of the motor.

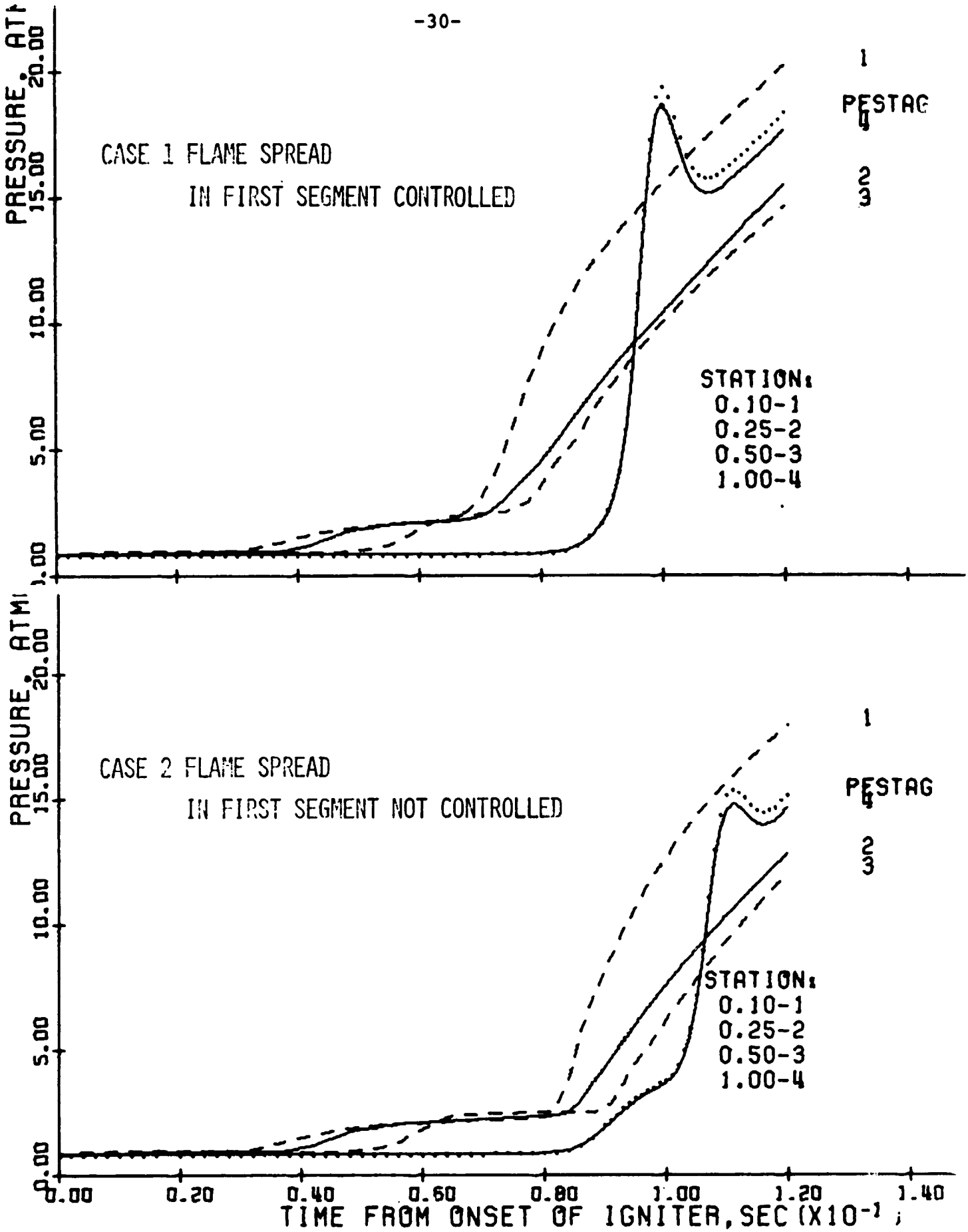

Fig. 8 Pressure vs time at five axial stations showing how flame spreading rate in the first segment alters the flow field development.

affects the magnitude of the thrust overshoot. Apparantly, if the igniter gases lead (by a sufficient period) the gases from the head-end segment, the F_{dyn} contribution is diminished and the effect of the strong longitudinal pressure wave is attenuated.

The dynamic thrust component has the proper trends with respect to the observed p and F vs t for DM1. However, net thrust measured for DM1 is the resultant of fluid flow dynamics as well as the dynamics of the motor case axial expansion and axial movement of the large propellant masses. Thus, the values of F_{net} for Cases 1 and 2 cannot be compared directly to the measured thrust values. After the Thiokol/Wasatch personnel complete their calculations of the case and propellant dynamics, the net resultant forces at the load cell can be approximated.

The important conclusions from the Case 1 and 2 calculations are:

1) The time period of the dynamic thrust coincides with the initial thrust rise and decay measured for DM1.
2) The overall flame spreading rate and dynamic thrust contributions are significantly affected by ignition and flame spreading of the first segment.
3) Longitudinal wave action within the chamber can produce accelerations in thrust similar to those noted in Fig. 2.
4) The modified program is an effective means of evaluating methods of tailoring the rate of thrust increase during the start up transients.

REFERENCES

1. Caveny, L. H. and Kuo, K. K., "Ignition Transients of Large Segmented Rocket Boosters," Apr. 1976, NASA Contractor Report to be published by NASA-George C. Marshall Space Flight Center.

2. Thurston, J. R., Personal Communication, Thiokol Corp., Wasatch Division, 5 March 1976.

Nomenclature for Analysis of Dynamic Thrust

A = area

$\vec{b}(t)$ = local boundary velocity which may vary over the surface S

$C_{F\lambda m}$ = thrust coefficient with losses taken into account

F = thrust

$\vec{G}(\vec{x},t)$ = body force (like gravity, electric field, etc.)

$\hat{n}$ = outward unit normal vector to the surface

p = pressure, static pressure unless designated as stagnation pressure

$S(t)$ = bounding surface

T = force

$\vec{T}(\hat{n},\vec{x},t)$ = surface force. Tensor, depends on orientation of the surface element defined by $\hat{n}$ (generally pressure, friction or thrust reaction in a test stand).

t = time

$\vec{u}(\vec{x},t)$ = velocity of any material element inside V (may be a gas element, a motor case element, or a propellant element).

$V(t)$ = a moving volume (not necessarily a material volume).

v = control volume

x = axial distance from head end

ϵ = movement of head end of motor

η = any summable continuous function

ρ = density

Subscripts

am = ambient

case = case

dyn = dynamic

ex = exit plane of nozzle

g	=	gases in rocket chamber
stag	=	stagnation
t	=	throat
pr	=	propellant
port	=	port area
x	=	axial direction

☆ U.S. GOVERNMENT PRINTING OFFICE 1978—740-193/366 REGION NO. 4